INSTITUTE OF PHYSICS PUBLISHING JOURNAL OF PHYSICS D: APPLIED PHYSICS

J. Phys. D: Appl. Phys. **37** (2004) 1137–1144 PII: S0022-3727(04)71451-5

Investigation of temperature control parameters for inductively heated semi-solid light alloys using infrared imaging and inverse heat conduction

A Bendada[1], **C Q Zheng and N Nardini**

National Research Council Canada, Industrial Materials Institute, 75 de Mortagne Boulevard, Boucherville, Quebec J4B 6Y4, Canada

E-mail: akim.bendada@imi.cnrc-nrc.gc.ca

Received 4 November 2003
Published 17 March 2004
Online at stacks.iop.org/JPhysD/37/1137 (DOI: 10.1088/0022-3727/37/7/030)

Abstract

In semi-solid die-casting, a metallic billet is first heated in an induction furnace until it reaches a semi-solid state (partially liquid and partially solid). Then, it is injected into a die and kept there until it is solidified. Subsequently, the die opens, the part is ejected and the cycle starts again. The liquid–solid fraction and its spatial distribution within the billet at the end of the heating phase are of prime importance for the success of the process and the quality of the final product. These parameters are strongly correlated with temperature gradients within the billet and their evolution in time through the heating cycle. There is presently no inspection method that could reasonably be used to control the billet temperature in a production environment. In this work, we investigate the suitability of using infrared thermography to meet the heating requirements. With this technique, it is possible to non-intrusively monitor the temperature distribution on the entire surface of the billet and to obtain information on how thermal energy is dissipated. Moreover, with the combination of surface infrared measurements and inverse heat conduction formalism, it is also possible to recover some information about the temperature distribution inside the billet. Effects of some process operating conditions such as heating power magnitude, power input cycles, location of the billet inside the induction coil, and the coil overhang are considered and discussed.

1. Introduction

The semi-solid forming process offers several advantages as compared to conventional casting of fully liquid alloys. These advantages include a lower shrinkage due to lower processing temperature and a higher viscosity which allows non-turbulent flow at higher filling rates than possible with fully liquid alloys. This results in an excellent dimensional repeatability, tight tolerances, an excellent surface finish, a low level of porosity as well as a very fine microstructure [1–4].

Rather than using fully liquid alloys as in the conventional die-casting, the semi-solid forming process uses alloys that are typically 40% liquid and 60% solid. At such a liquid fraction, the rheological properties of the semi-solid alloy are very sensitive to variations in the liquid phase portion [5]. Thus, it is extremely important to maintain the liquid fraction in a very narrow threshold and to ensure its uniform distribution throughout the heated billets prior to their injection into the die. The heating procedure must then be accurately controlled to achieve a uniform temperature in the billets and the required optimum liquid fraction for casting. Furthermore, alloys destined for semi-solid forming are specially treated to have a very uniform fine-grained microstructure. To maintain this initial microstructure, the heating process must be relatively fast as well [3, 6].

[1] Author to whom any correspondence should be addressed.

The commonly used technology for achieving these criteria in commercial production applications is induction heating. Billets of cylindrical shape are placed on vertical individual ceramic pedestals and subsequently introduced into cylindrical coils to be inductively heated. However, induction heating has the drawback of being non-uniform, which yields strong top-to-bottom and surface-to-core thermal gradients within the billet [7, 8].

In the majority of the studies already undertaken, temperature control was performed using thermocouples [7, 9, 10]. The thermocouples were either welded or in free contact at many locations on the surface and/or inside the work piece. But on the production floor, the use of thermocouples, or any other invasive technique, was not very practical due to the nature of the semi-solid process itself. To overcome the invasive aspect of thermocouples, some researchers have equipped their heating stations with optical fibre thermometers [11]. However, this solution was limited to local temperature measurements on the surface and was emissivity dependent. Emissivity is required to convert the output of the photon detector into a value representing the object temperature. During induction heating, billet emissivity is not predictable since it is affected by several factors such as temperature, alloy oxidation, surface texture and alloy grade.

To avoid the limitation to local or pointwise measurements, we propose in this work to use infrared thermography. This technique has the advantage of providing high-resolution temperature cartography of the entire surface of the work piece. However, it also requires the emissivity of the material and is limited to surface measurements. To bypass the emissivity issue, we use a procedure that consists in coating the billet with a high-emissivity paint, which is insensitive to the above-mentioned factors. However, this method has the drawback of changing the radiative properties of the billets which are therefore different from those encountered during normal operation. The extent to which the quantitative results stemming from the coating method are representative of real processing is very difficult to evaluate without an accurate comparative measurement method or a theoretical modelling of the heating phase. Modelling can show how temperature within the billet is sensitive to emissivity variations caused by surface oxidation and roughness change during heating. Nevertheless, the coating method is able to provide useful qualitative knowledge about eventual uneven temperature profiles resulting from non-uniform heating. On the other hand, to overcome the limitation of thermography to surface measurements, an inverse procedure is used to predict the temperature distribution along the radius of the billet from the measured surface infrared data.

The results of heating trials that illustrate the influence of the undesirable phenomena and process parameters on the temperature distribution are presented. Other experiments carried out to alleviate the thermal gradients within the billet and reduce the heating time are also reported.

2. Experimental apparatus

The material used in the experiments was A356 aluminium alloy (Al-7.0% Si-0.35% Mg-0.2% Cu-0.2% Fe-0.1% Mn-0.1% Zn-0.05% Sr) supplied by Ormet Corporation. The workable temperature range for this alloy is generally within the range 580–585°C. The thermophysical properties of the material at the solid phase are temperature dependent and are given in table 1. The aluminium billets were cut in cylinders 3″ (76.2 mm) in diameter and 6″ (152.4 mm) in height from long bars.

Table 1. Thermophysical properties of A356 aluminium alloy.

Density (kg m^{-3})	$-0.208T$ (°C) + 2680.0
Specific heat (J kg^{-1} °C^{-1})	$0.454T$ (°C) + 904.6
Thermal conductivity (W m^{-1} °C^{-1})	$0.04T$ (°C) + 153.1
Solidus temperature (°C)	550
Liquidus temperature (°C)	615

The trials were carried out in a three-coil induction-heating unit manufactured by Induction Heating Specialists (IHS). The billets were placed on ceramic pedestals and then moved up into the cylindrical coils to be inductively heated. Thin refractory cylinders stand between the coils and the billets. The heating station was equipped with an automatic moving two-finger thermocouple for measuring the temperature at the centre of the top surface of the billet. The frequency of the induction heating current was measured during the experiments and was found around 1 kHz for the range of power magnitudes employed in this work. Power adjustment from the lowest magnitude to the highest magnitude was realized by using a button graduated in arbitrary unit from 300 to 1000. Absolute power levels were inaccessible on this machine version.

Billet surface temperature was recorded with an AGEMA 900 LW infrared camera. This was sensitive in the spectral band 8–12 μm, had a temperature resolution of 0.08°C at 30°C, an accuracy of 1% from 80°C up to 2000°C, and a repeatability of 0.5% in the same range. A high-emissivity black paint was used to avoid the problem of emissivity variations with temperature and oxidation during heating. The paint was resistant to temperatures up to 650°C. Its emissivity in the sensitive band of the infrared camera was determined using a blackbody source to be $\varepsilon = 0.94$.

3. Top-to-bottom thermal gradients

The top-to-bottom temperature profile is essentially due to the distortion of the electromagnetic field at the ends of the work piece and to additional heat losses in those areas as compared to the central one. These end effects can result in either overheating or underheating of the billet ends and are related to several factors such as the frequency and the magnitude of the coil current, the billet-to-coil free space, the coil overhang: the distance between the billet end and the coil end (figure 1), the billet material and the pedestal material. It is worth noting that temperature non-uniformity in the billet may also result from other undesirable effects such as the 'elephant foot' phenomenon [12]. The latter takes place due to the migration of the liquid phase under gravity to the bottom of the billet.

Electromagnetic end effects may be illustrated by the curves in the lower diagram of figure 1. Basically, the electromagnetic end effect in the billet is defined by three variables: (1) the 'skin effect' R/δ where R is the billet radius and δ is the skin depth defined in section 4 below; (2) the

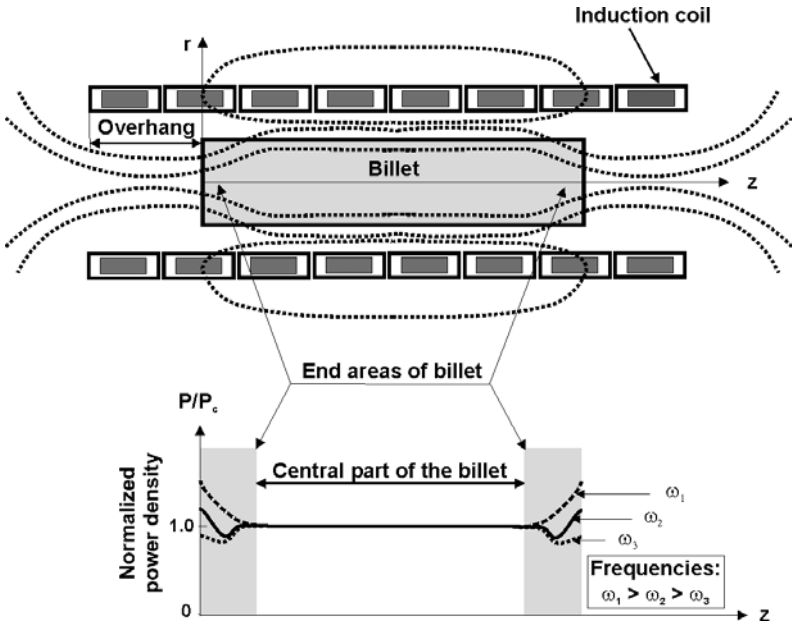

Figure 1. Sketch of induction heater and power density distribution along the billet length. Electromagnetic end effects are illustrated by the curves in the lower diagram of the figure (P_c is the surface power density in the central part of the billet).

coil overhang σ; (3) the billet-to-coil air gap R_{coil}/R where R_{coil} is the inside radius of the coil. Figure 1 shows typical electromagnetic field and power density distributions in the areas located at the ends of the billet. Inappropriate choice of the above mentioned factors could lead to underheating or overheating of the ends of the billet. Studies show that the electromagnetic end effect area extends toward the central region of the billet (figure 1) no further than one time of the billet radius (typically 0.4–0.7 of the billet radius) [8]. Higher frequency and large coil overhang will lead to a power surplus in the end areas of the billet. As a result, significant overheating and even melting may take place in those areas. A low frequency and small coil overhang will cause a power deficit at the ends of the billet, which will, therefore, be underheated. It should be mentioned that a uniform power distribution along the billet would not correspond to its uniform temperature distribution. This is due to additional heat losses at the billet end areas compared to its central part. By selecting suitable design parameters, it is possible to obtain a situation where the additional heat losses at the ends of the billet are compensated for by the additional power (power surplus) due the electromagnetic end effect. This will allow obtaining a reasonable uniform temperature distribution within the billet at the ends as well as at the centre.

To evaluate the evolution in time of the effect of electromagnetic distortions at the billet ends, the billet was moved out twice (<2 s) from the coil so that the camera could capture the image of the painted vertical surface. The two measurements were made when the temperature read by the two-finger thermocouple at the centre of the top surface of the billet was 300˚C and 550˚C, respectively. Thermal frames recorded at an experiment carried out with a high-heating power show in figures 2 and 3 that the billet ends were overheated compared to the central area. It could also be noted that the temperature profiles were not perfectly symmetrical, especially at the beginning of heating (figure 2) where the

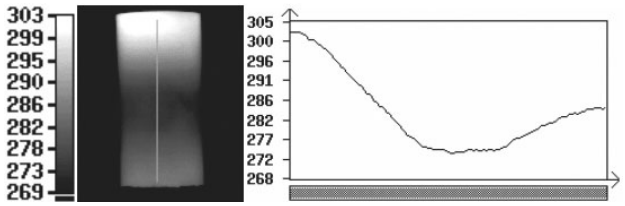

Figure 2. Infrared image and a top-to-bottom temperature profile showing the effect of the distortion of the electromagnetic field near the billet ends during a high-power heating cycle. These data refer to the time the thermocouple at the centre of the top surface of the billet indicated a temperature of 300˚C.

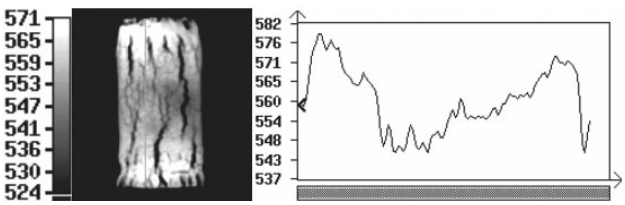

Figure 3. Infrared image and a top-to-bottom temperature profile showing the effect of the distortion of the electromagnetic field near the billet ends during a high-power heating cycle. These data were recorded when the thermocouple at the centre of the top surface of the billet indicated a temperature of 550˚C.

billet top end was more overheated than the bottom end. This was somewhat surprising, since the top surface was normally submitted to more heat losses than the billet base and the lateral free convection did not strongly affect the shape of the top-to-bottom temperature profile. The latter asymmetric vertical heating concern was explained by a billet located off-centre inside the inductive coil. Indeed, after checking the heights of the billet pedestal and the inductive coil, we found out that the billet was improperly positioned 20 mm below the coil centre. Furthermore, it was also observed

from figure 3 that near the end of the heating process, the billet base temperature caught up progressively with the top temperature, but the coldest area was still off-centre. This was due to the development of the 'elephant foot' effect at the billet base as shown in the infrared image of figure 3. The existence of the 'elephant foot' phenomenon was an indication that portions of the billet have already reached a semi-solid state and the liquid eutectic phase was migrating to the base under gravity. This effect would result in an uneven coupling with the electromagnetic field along the billet height and thus aggravating the 'elephant foot' effect. It might be noted that fluctuations in the temperature profile reported in figure 3 were not due to real temperature variations; they were the result of the appearance of local cracks in the black paint at the billet surface leading to emissivity variations on the surface.

Another key parameter that affects the top-to-bottom temperature distribution is the coil overhang. The IHS heating station allows the adjustment of three different coil lengths: 6″ (152.4 mm), 11″ (279.4 mm), and 17″ (431.8 mm). The previous results reported in figures 2 and 3 were obtained when a 17″ coil length was employed in order to assess the overhang influence, another experiment was performed with a high-power magnitude and a coil length set to 6″, the same length as the billet height. In this experiment, the billet and the coil locations were kept unchanged and their centres were still separated by 20 mm. Figure 4 illustrates a thermal image that exhibits a shape of a top-to-bottom temperature profile completely different from those already reported in figures 2 and 3. This time, the temperature decreased in a quasi-monotonic way from the top toward the bottom of the billet. The latter temperature profile clearly confirmed the effect of the non-superimposition of the billet and electromagnetic field midpoints. We performed another test with the billet mid-point well centred inside the inductive coil. Figure 5 shows an example of the top-to-bottom temperature distribution obtained with the new

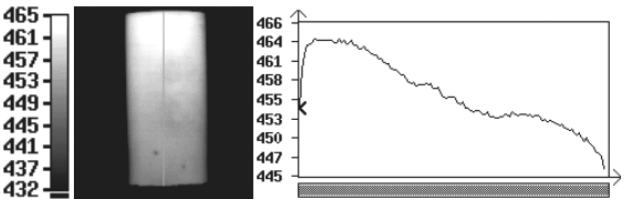

Figure 4. Infrared image and a top-to-bottom temperature profile showing the effect of a smaller overhang on the distortion of the electromagnetic field near the billet ends during a high-power heating cycle. The asymmetry of the temperature profile is caused by the fact that the billet centre was placed ∼20 mm below the coil centre line.

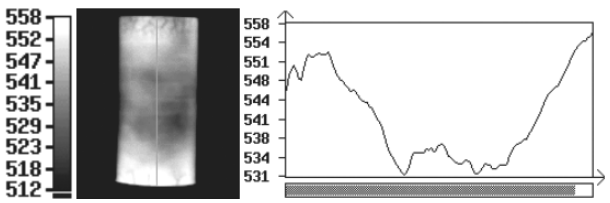

Figure 5. Infrared image and a top-to-bottom temperature profile recorded for the same overhang size as for figure 4 but this time the billet was moved up into the coil until superimposition of the billet and coil mid-points.

adjustment of the pedestal. The temperature profile was more symmetrical than previously observed. It might be noted however that the bottom was slightly more overheated than the top, which was in good agreement with the higher heat losses at the top and the 'elephant foot' effect at the bottom. We mention for reference that the time that was needed to reach the solidus temperature while using a small coil length was too long (25 min) compared to the previous large coil length configuration (4 min). The optimum heating time that is recommended in the literature for a 3″-diameter billet is 5 min [8]. The larger is the billet diameter, the higher is the optimum recommended heating time. As an example, for a 4″-diameter billet, the optimum recommended heating time is 8 min [8]. Slower heating ensures that sufficient time is provided for the heat to conduct from the surface to the centre of the billet, resulting in a more uniform surface-to-core temperature profile.

4. Surface-to-core thermal gradients

During induction heating, energy is transferred from the coil to the billet by an alternating electromagnetic field. The induced electromagnetic force produces a current circulation in the billet, which generates heat by Joule effect. The current, and therefore the generation of heat, is concentrated at the surface and its density falls off nearly exponentially with distance from the outer surface to the core:

$$I = I_0 \exp\left(-\frac{R-r}{\delta}\right) \tag{1}$$

where I_0 is the current density at the outer surface, R is the outer radius of the billet, r is the radial distance and δ is usually referred to as the penetration depth or the skin depth and is given by

$$\delta = \sqrt{\frac{2\rho}{\mu\omega}} \tag{2}$$

In this expression, ω is the angular frequency of the primary current, μ is the magnetic permeability of the billet material and ρ is its electrical resistivity. In practice, approximately 86% of the heating energy is concentrated in the skin depth [7, 8]. Heat concentrated near the surface is then conducted toward the centre of the billet and at the same time lost to the environment through convection and radiation. It should be pointed out here that because of the latter simultaneous phenomena, conduction, convection, radiation, Joule effect, an exponential current density distribution along the radial direction of the billet would not necessarily yield an exponential temperature distribution.

To investigate the influence of the 'skin effect' on the surface-to-core thermal gradients within the billet, two approaches were undertaken. The first approach was based on the use of the infrared camera to directly obtain the radial temperature distribution at the end of the billet, while the second approach was based on the use of an inverse problem formulation to recover the radial temperature distribution far from the ends. For both approaches, the effect of the heating power on the radial distribution of the temperature within the billet was investigated by using three different power magnitudes: low, medium and high.

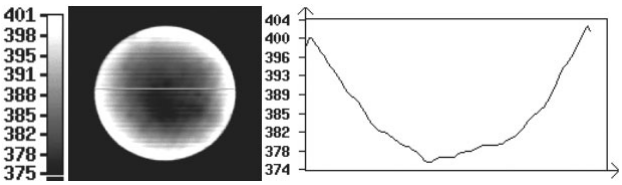

Figure 6. Infrared image and a surface-to-core temperature profile showing the 'skin phenomenon' on the top surface of the billet during a high-power heating cycle. These data were recorded in the middle of the heating cycle.

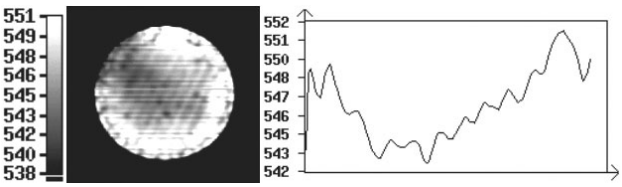

Figure 7. Infrared image and a surface-to-core temperature profile showing the 'skin phenomenon' on the top surface of the billet during a high-power heating cycle. These data were recorded just before the end of the heating cycle.

In the first approach, images of the top surface of the billet were monitored using a gold-coated mirror (Edmund Scientific Company) placed at the top end of the induction coil at 45° to reflect the image out to the infrared camera. In this experiment, only the top surface was black painted in order to keep the test conditions as close as possible to the normal operating process, while all the remaining billet sides were kept uncoated. Figures 6 and 7 show two infrared images of the billet top surface recorded near the beginning and the end of the heating cycle, respectively, when a high-heating power was utilized. The 'skin effect' can be clearly observed on those images and the extracted surface-to-core temperature profiles. This phenomenon was more significant in the beginning of the heating phase (figure 6) where thermal gradients were up to $0.70^{\circ}\mathrm{C\,mm^{-1}}$, while near the end of the heating (figure 7), the gradients were strongly reduced to about $0.20^{\circ}\mathrm{C\,mm^{-1}}$. This gradient evolution was likely due to the growth of the 'penetration depth' during the heating cycle since the electrical resistivity of aluminium was very sensitive to temperature variations and could increase more than three times its initial value at room temperature [8]. Furthermore, when the solidus temperature was reached, the heat generation was used up in melting the material rather than in further increasing the temperature.

While the high-power experiment gave a maximum temperature gradient of $0.70^{\circ}\mathrm{C\,mm^{-1}}$, medium- and low-power trials showed that radial thermal gradients during the heating cycle might reach $0.40^{\circ}\mathrm{C\,mm^{-1}}$ and $0.18^{\circ}\mathrm{C\,mm^{-1}}$, respectively. As noted previously, the duration required to reach the semi-solid state must be as short as possible to preserve the initial microstructure of the billet material. In parallel to thermal gradients analysis, the duration of the heating cycle was also analysed for the three heating powers employed. The experiments revealed that the larger the overhang the shorter the heating time. The heating durations were 4 min for the high power, 6 min for the average power, and 12 min for the low power.

In the second approach, the temperature distribution along the radius of the billet before the alloy started to melt (one-phase model to two-phase model is the subject of on-going research) was estimated from surface infrared data monitored far from the billet ends using an inverse heat conduction method. The method was applicable either for cases where the electromagnetic end effects are not significant or at locations far from the ends where these undesirable phenomena were negligible. It should be pointed out here that the electromagnetic end effects are in general easier to control than the 'skin effect'. By a proper choice of set-up parameters, it is possible to obtain a situation where the additional heat losses at the ends of the billet are compensated for by the additional energy (overheating) due to the electromagnetic end effects. This will allow a reasonably uniform temperature profile along the height of the billet to be achieved [8]. The detailed description of the adopted method has been presented elsewhere [13–15], and only a brief account is given here. The physical definition of the inverse problem was to reconstruct the unknown initial temperature distribution by measuring the surface temperature of the billet as a function of time after heating stopped. The surface temperature of the billet was readily measurable and was a direct consequence of the internal temperature distribution. By using different portions of the time response data at the surface, the evolution in time of the temperature profile inside the billet could be predicted.

The experimental procedure was as follows. First, the refractory cylinder inside the heating coil was taken away so that the camera could capture the image of the vertical surface through the gaps between the coil turns. Then, the infrared camera was turned on but was not recording. At 200 s after the beginning of the heating, the induction power was turned off and the camera started to record the surface temperature cooling with time. The time, at which the measurement was performed, namely 200 s, corresponded to the time the surface temperature read by the infrared camera was around 500°C and the billet material was still solid (as shown in table 1, the solidus temperature for the A356 alloy is 550°C). The temperature from a single spot on the side surface of the billet was extracted from the infrared sequences and used to reconstruct the temperature distribution in the radial direction of the billet. The measurement spot was located at the centre of a small black painted area, 1 cm × 1 cm. Only that area was coated with the high-emissivity paint in order to keep the radiative conditions during testing as close as possible to those that would occur during normal processing. A typical surface temperature data for the high-power experiment is illustrated in figure 8. Surface temperature curves were extracted from the mid-height of the billet far from its overheated ends.

Figure 9 shows the predicted surface-to-core profiles for the three heating power magnitudes. As expected, the higher was the power, the larger was the deviation between the surface and core temperatures. The deviation between the extreme temperatures was 17°C, 15°C and 13°C, respectively. It is also noted that the shape of the profile changed from one power level to another. This was a result of the mutual competition between the 'skin effect', the heat conduction and the heat losses at the surface. For high-power level, the penetration depth was small so that the heat source from induction heating was concentrated near the skin resulting in a high temperature at the surface and

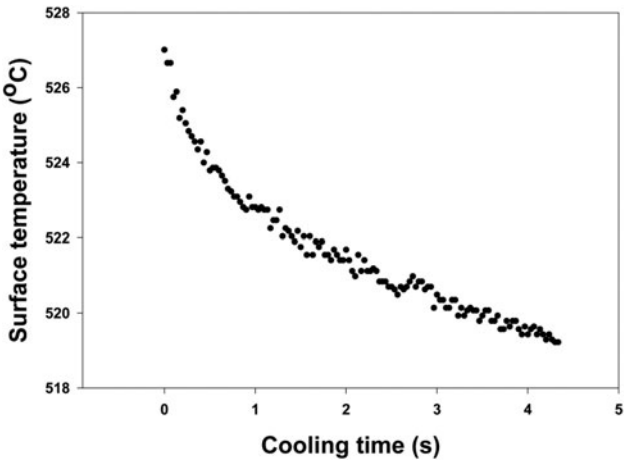

Figure 8. A typical surface temperature against time curve at one point of the central part of the billet after the heating was stopped. The data were recorded during a high-power heating experiment.

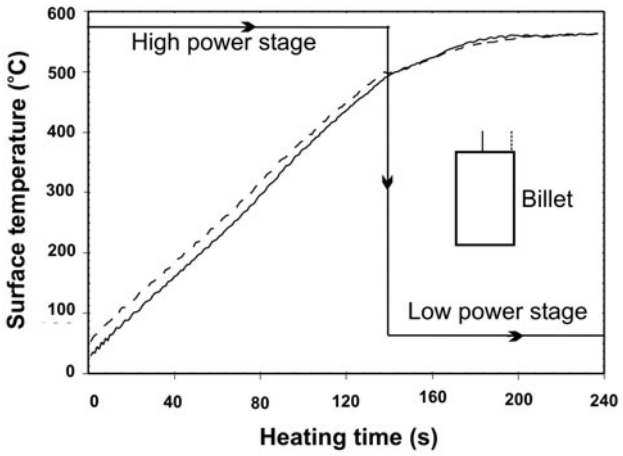

Figure 10. The power input profile for a two-stage heating cycle and the temperature variation on the centre (——) and the edge (- - - -) of the top surface of the billet as indicated by the sketch in the figure. The heating power was lowered 140 s after heating had started.

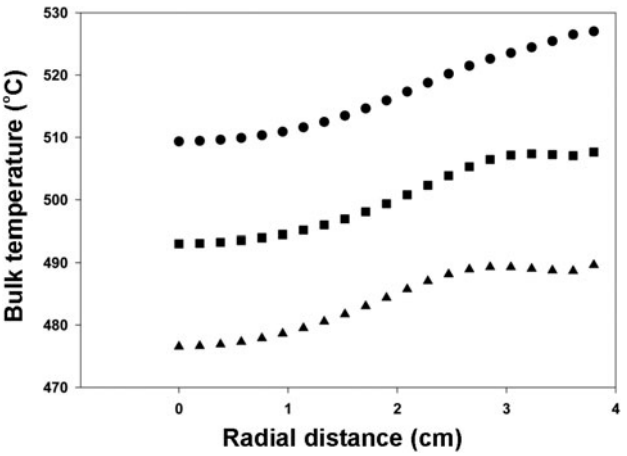

Figure 9. Recovered radial temperature profiles using the surface temperature versus time data; (●) refers to high-power heating; (■) refers to a medium-power heating; (▲) refers to a low-power heating.

the heat was transferred to the centre by conduction. The high thermal conductivity of aluminium caused thermal gradients to be nearly constant; the temperature increased almost gradually from the centreline to the surface. In contrast, for medium- and low-power levels, the electromagnetic depth was larger giving rise to a heat source at a point between the surface and the centre. Heat was then conducted toward both the surface due to surface cooling and toward the centre. This resulted in a temperature plateau near the surface for both cases and the length of the plateau region was somewhat larger for lower power. However, a slight rise in temperature was apparent towards the edge of the billet for both the medium- and low-power profiles. This was caused by convective and radiative heat losses at the outer surface of the billet. Because of the high thermal conductivity of the A356 alloy, the competition between heat conduction within the billet and heat losses at the surface led to only weak temperature gradients in the edge region. On the contrary, the curves reported in figure 9 do not show any sudden rise of the temperature near the centreline ($r = 0$) of the billet; the symmetry of the billet and the inductive coil caused the radial heat flux crossing the centreline to be zero. Even though it was shown that the inversion procedure could provide a fairly reliable temperature prediction within a few percent, caution should be taken not to over-interpret the results, especially small-scale details.

5. Control of thermal gradients via two-stage heating experiments

The heating procedure must be carefully controlled to achieve a uniform temperature distribution and the required liquid–solid fraction in the heated billets in the shortest possible heating duration. One approach to reach this aim is to divide the heating cycle into several power input stages starting with a high-power heating stage then lowering it sequentially in the subsequent stages. The initial high-power stage leads to a strong uneven surface-to-core temperature profile, but this unevenness disappears by conduction in the subsequent low-power homogenizing stages. In the present study, the heating process was controlled by the power input and time via two heating stages and was controlled by using infrared images of the billet top surface. The experimental procedure aimed to eliminate thermal gradients only along the radius of the billet. Top-to-bottom temperature gradients were not considered here since they could be eliminated by an appropriate choice of the heating parameters.

Two trials were carried out. In the first trial, switching from the high-power stage to the low-power stage was performed 140 s after the heating had started. In the second trial, the heating power was lowered to the low-power stage 205 s after the heating had started. Figures 10 and 11 show the power input profiles with the heating duration for the two stages, and the temperature variation during heating on the centre and the edge of the billet top surface. The small sketch of the billet plotted in each figure shows exactly where the two temperatures were monitored. The recovered temperature variation in both experiments indicated that there was only very slight temperature difference between the outer surface

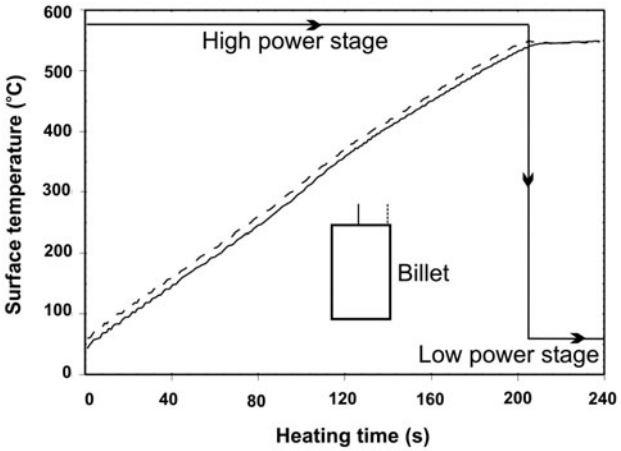

Figure 11. The power input profile for a two-stage heating cycle and the temperature variation on the centre (——) and the edge (- - - -). The heating power was lowered 205 s after heating had started.

Figure 12. Illustration of the 'elephant foot' effect after the first two-stage heating test (switching time at 140 s).

and the centre at the end of heating (1–2˚C). The time of power switching did not lead to a significant difference in the radial temperature profile in the two tests. However the result in both cases was better (<2˚C) than thermal gradients observed previously in a one high-power input stage (>8˚C, figure 7). After completion of heating, the billets were moved out of the coil. In the first experiment, a significant 'elephant foot' phenomenon was clearly observed at the bottom of the billet (figure 12); while in the second experiment, a relatively straight wall was produced, the billet was quite soft, easily cut like butter and presented no handling problems (figure 13). These results revealed that though the temperature on the top surface after the heating was almost uniform for the first billet, the 'elephant foot' effect could not be prevented. The time at which the power had to be lowered had a major impact on the development or not of an 'elephant foot'.

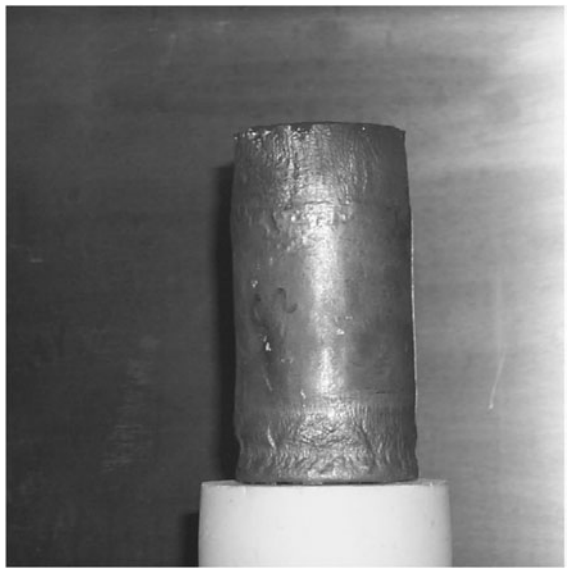

Figure 13. Image of the semi-solid billet keeping its initial shape after the second two-stage heating test (switching time at 205 s).

6. Summary

It was shown that though infrared thermography was limited to surface temperature measurement and was emissivity dependent, it could still provide important information about the induction heating phase in semi-solid casting.

Infrared images recorded on the billet top surface illustrated clearly the 'skin effect' and showed that it was more significant at the beginning of heating than at the end. This was likely related to the growth of the 'penetration depth' throughout the heating cycle. Moreover, an inversion algorithm was utilized to predict the surface-to-core internal temperature profile using infrared data measured at the billet surface. Reasonable temperature profiles were obtained for different power heating magnitudes.

Infrared measurements carried out on the vertical surface of the billet demonstrated that the top-to-bottom temperature profile was not symmetrical with respect to the mid-height of the billet. The billet was more overheated at the top end than at the bottom end. A thorough check of the heating system revealed that the asymmetry of the electromagnetic field was caused by the fact that the billet was placed off-centre inside the induction coil. After superimposing the billet centre with the coil centre, a symmetrical temperature distribution was observed. The influence of the overhang was investigated as well. It was noted that the shape of the top-to-bottom temperature profile changed and also the heating duration increased when the overhang reduced.

Two-power-stage heating trials were undertaken to alleviate the thermal gradients within the billet before the end of heating. Temperature gradient control was performed on the top surface of the billet. The results showed that reducing thermal gradients on the top surface could not be the only criterion to obtain a uniform temperature distribution within the entire billet. Time at which the heating power had to be reduced from a high-power stage to a low-power stage was revealed a key parameter that had a crucial impact on temperature uniformity.

References

[1] Midson S and Brissing K 1997 *Mod. Cast.* **2** 41
[2] Nussbaum A I 1996 *Light Met. Age* **6** 6
[3] Boylan J 1997 *Adv. Mater. Processes* **10** 27
[4] Young K P and Brissing K 1996 *Die Casting Eng.* **3** 12
[5] Flemings M C 1991 *Met. Trans.* A **22** 957
[6] Valencia J J, Friedhoff T G, Creeden T P and Cardella J J 1998 *Proc. 5th Int. Conf. on Semi-solid Processing of Alloys and Composites* (Golden, CO: Colorado School of Mines) p 397
[7] Kapranos P, Gibson R C, Kirkwood D H and Sellars C M 1996 *Proc. 4th Int. Conf. on Semi-solid Processing of Alloys and Composites* (Sheffield, UK: University of Sheffield) p 148
[8] Midson S, Rudnev V and Gallik R 1998 *Proc. 5th Int. Conf. on Semi-solid Processing of Alloys and Composites* (Golden, CO: Colorado School of Mines) p 497
[9] El-Kaddah N, Craen R and Loue W 1998 *Proc. Int. Conf. on Light Metals* (San Antonio, TX: Minerals, Metals and Materials Society) p 1097
[10] Kirkwood D H 1998 *Proc. 5th Int. Conf. on Semi-solid Processing of Alloys and Composites* (Golden, CO: Colorado School of Mines) pp xxxiii–xl
[11] Lasday S B 1995 *Indust. Heating* **6** 28
[12] Midson S, Rudenev V and Gallik R 1999 *Indust. Heating* **1** 37
[13] Nguyen K T and Bendada A 2000 *Modelling Simul. Mater. Sci. Eng.* **8** 857
[14] Bendada A and Nguyen K T 1999 *Proc. 3rd Int. Conf. on Inverse Problems in Eng.* (Port Ludlow, WA: American Society of Mechanical Engineers) p 355
[15] Bendada A and Nguyen K T 2001 *Proc. 27th Annual Review of Progress in Quantitative Nondestructive Evaluation* (Ames, Iowa: American Institute of Physics) p 1562